Journal of Loss Prevention in the Process Industries 38 (2015) 24–38

Contents lists available at ScienceDirect

Journal of Loss Prevention in the Process Industries

journal homepage: www.elsevier.com/locate/jlp

Effect of CO_2 corrosion behavior of mild steel in oilfield produced water

Aprael S. Yaro [a], Khalid R. Abdul-Khalik [a], Anees A. Khadom [b, *]

[a] Chemical Engineering Department, College of Engineering, University of Baghdad, Aljadrea, Baghdad, Iraq
[b] Chemical Engineering Department, College of Engineering, University of Diyala, Baquba City, Diyala, Iraq

ARTICLE INFO

Article history:
Received 23 March 2015
Received in revised form
18 July 2015
Accepted 20 August 2015
Available online 28 August 2015

Keywords:
Alloy
Corrosion
Electrochemical techniques
X-ray diffraction topography

ABSTRACT

The corrosion rates of API X65 mild steel alloy in CO_2 – containing produced water have been studied by weight loss technique, potentiodynamic polarization technique and characterization of the corroded surface techniques. The effect of temperature, speed of rotation, pH and acetic acid concentration were studied. The optimum condition in presence and absence of protective film were also addressed. The kinetic parameters and reaction behavior were discussed in details. Corrosion rates increases with increasing temperature, acetic acid concentration, and speed of rotation, and decreased with increasing solution pH. The primary corrosion product of API X65 mild steel is ferrous carbonate ($FeCO_3$) at high temperatures, high pH's (alkaline media) and absence of acetic acid, which could act as a protective film so that CO_2 corrosion rate can be reduced.

1. Introduction

Carbon dioxide (CO_2) corrosion is one the most studied form of corrosion in oil and gas industry. This is generally due to the fact that the crude oil and natural gas from the oil reservoir/gas well usually contains some level of CO_2. The major concern with CO_2 corrosion in oil and gas industry is that CO_2 corrosion can cause failure on the equipment especially the main down hole tubing and transmission pipelines and thus can disrupt the oil/gas production. The presence of carbon dioxide (CO_2) and free water can cause severe corrosion problems in oil and gas pipelines. Internal corrosion in wells and pipelines is influenced by temperature, CO_2 content, water chemistry, flow velocity, oil or water wetting and composition and surface condition of the steel. A small change in one of these parameters can change the corrosion rate considerably, due to changes in the properties of the thin layer of corrosion products that accumulates on the steel surface (Nyborg, 2010). When corrosion products are not deposited on the steel surface, very high corrosion rates of several millimeters per year can occur. The corrosion rate can be reduced substantially under conditions where iron carbonate ($FeCO_3$) can precipitate on the steel surface and form a dense and protective corrosion product film. This occurs more easily at high temperature or high pH in the water phase (Koteeswaran, 2010). High temperature increases the rate of reaction that produces the protective corrosion products layer which reduces corrosion rates. While high pH (low acidity) reduces the descaling of corrosion products layer which yields low corrosion rate. CO_2 corrosion, or "sweet corrosion," of carbon steel is not a new problem. It was first recorded in the U.S. oil and gas industry in the 1940s, followed by several studies since then (Garsany et al., 2002). Dry CO_2 gas by itself is not corrosive at the temperatures encountered within oil and gas production. It needs to be dissolved in an aqueous phase to promote an electrochemical reaction between steel and the contacting aqueous phase. CO_2 is soluble in water and brines. However, it should be noted that it has a similar solubility in both the gaseous and liquid hydrocarbon phases. Thus, for a mixed-phase system, the presence of hydrocarbon phase may provide a ready reservoir of CO_2 to partition into the aqueous phase. CO_2 is usually present in produced fluids. Basically, CO_2 corrosion is an electrochemical process of a multistep nature between the corrosive species resulting from CO_2 dissolution and the dissolvable phases in the steel. A great effort has been devoted to determine the governing anodic and cathodic reactions and to determine the key species involved. Organic acids, especially the weak one, are known to affect the rate of CO_2 corrosion to a very large amount. Acetic acid is one of these acids. Hedges and McVeigh, (Hedges and McVeigh, 1999) published results on acetates role in CO_2 corrosion. Experiments using both HAc and sodium acetate as a source of acetate

* Corresponding author.
E-mail address: aneesdr@gmail.com (A.A. Khadom).

http://dx.doi.org/10.1016/j.jlp.2015.08.003
0950-4230/

ions in various media (3% NaCl and two synthetic oilfield brines) were performed using rotating cylinder electrodes. Both sources of acetate ions were shown to increase the corrosion rate. Gunaltun, (Gunaltum and Larrey, 2000) reported that very few systematic studies have been performed in the laboratory. Little or no information exists about the basic effect of HAc on the anodic and cathodic reactions. Garsany et al., (Garsany et al., 2002) performed work using voltammetry to study the effect of acetate ions on the rates and mechanisms of corrosion using a rotating disc electrode (RDE) on film-free surfaces. Their voltammograms show two waves, which are attributed to hydrogen ion and HAc reduction on the steel surface. They argue that since HAc dissociation can occur very quickly it is not possible to distinguish the reduction of hydrogen ions from direct HAc reduction at the electrode surface. Joosten et al., (Joosten George et al., 2004) performed additional experiments using acetic acid, synthetic seawater, and an oil phase in glass cells. They found that acetic acid increased the corrosion rate by decreasing the pH. Sun et al., (Sun et al., 2003) recently published work using potentiodynamic sweeps to the study the effect of HAc on the cathodic and anodic reactions using a rotating cylinder electrode (RCE). Their work suggests HAc acts solely as an additional source of hydrogen ions. Dougherty, (Dougherty, 2004) reported a mild increase in the cathodic reaction in the presence of HAc although their results were not fully conclusive. The objective of this study is to investigate the effect CO_2 – mild steel corrosion in presence of free acetic acid. Corrosion rates will be evaluated at different operation conditions of temperature, speed of rotation, acid concentration, and pH. Two techniques were used to evaluate the corrosion rates. Furthermore, microscopic and surface studies were used to support the results. Mathematical and statistical analysis was a powerful way to correlate the dependent and independent variables and to evaluate the optimum conditions.

2. Experimental work

2.1. Weight loss and polarization tests

The corrosion behavior of API X65 mild steel alloys, used widely in oil and gas production and transport industries, was studied using weight loss and polarization technique in presence and absence of acetic acid in 3.5 wt.% NaCl of CO_2–saturated solution by bubbling CO_2 gas (>99.99%) at 1 bar for 1.5 h, at different temperatures (40, 50 and 60 °C), different pH's (3, 4 and 5), different HAc concentrations (1000, 2000 and 3000 ppm) and different speeds of rotation (1000, 1250 and 1500 rpm). In absence of acetic acid at different temperatures (65, 70 and 75 °C), different pH's (7.5, 8 and 8.5) and different speeds of rotation (1000, 1250 and 1500 rpm). The corrosive solution used in this work was 3.5 wt.% NaCl saturated with pure carbon dioxide CO_2 gas during 1.5 h prior the immersion of the metal samples. Weight loss technique is the widely used method for determining the corrosion rate. The corrosion of API X65 mild steel in CO_2 saturated, 3.5 wt. % NaCl solution was studied in presence and absence of acetic acid. 32 runs were carried out at desired different conditions. In addition to, 10 runs were performed in simulated brine and compared to 3.5 wt. % NaCl solutions saturated with CO_2 gas in presence and absence of acetic acid at different experimental conditions. A typical procedure adopted was as follows: a specimen of known surface area and mass is exposed to the test corrosive solution for a fixed period of time 3 h. The loss of a metal as a result of corrosion is then determined from the loss of mass in specimen after removal the corrosion products or other deposits from metal. Mass loss values are usually recorded together with the exposed surface area of the specimen and the period of the test. Frequently the data are expressed as mass loss per unit time per unit area, e.g. g/m^2 day (gmd). In this work, cylinder shape specimen of API X65 mild steel alloy with dimensions 2.03 cm outside diameter, 2.08 cm long and 0.13 cm thickness, exposing a surface area of about 13.27 cm^2 to corrosive media. Specimens were cleaned by washing with detergent and flushed with tap water followed by distilled water, degreased by benzene and acetone. Before each run, specimens of API X65 mild steel were abraded in sequence using emery paper of grade number 220, 320, 400 and 600, then washed with running tap water followed by distilled water then dried with clean tissue, degreased with benzene, dried, degreased with acetone, dried, and finally left in dissector over silica gel. A total of 36 test runs were carried out in presence and absence of acetic acid at different experimental conditions using potentiodynamic polarization technique. Tests were carried out using a glass cell of 2.5 L. The cell was equipped with eight holes, seven of them are used. One for the working electrode (mild steel cylinder). One had a cylindrical hole for mounting the lugging capillary prob., one for thermometer, one for the counter graphite electrode, one for pH probe and two for gas inlet and outlet. All potential values were measured in reference to saturated calomel electrode (SCE). The lugging capillary prob. was adjusted such that it was at a distance not more than 1 mm from the working electrode. The working electrode was (2.03 cm outside diameter x 2.08 cm long) API X65 mild steel alloy cylinder; this cylinder was fixed on brass zone on the shaft. Graphite electrode was used as a counter electrode has a dimension of (3.1 cm diameter × 4 cm long), two wires were connected to a cylindrical concentric graphite electrode, and then fixed within Teflon ring. The electrode was mounted directly to the working electrode. Saturated calomel electrode (SCE) was used as reference electrode. To ensure that KCl solution was saturated, a small amount of KCl (solid) was kept in the solution of (SCE) as long as the test. The cathodic polarization is carried out beginning from highest negative potential of (−1000 mV) until reaching the corrosion potential. The potential was changed (10–15 mV) for each step after a one-minute period, the current is recorded. While, the anodic polarization readings start at a potential resulting in a zero current density and is increased in a step of (10–15 mV) with recording of current at each step for one minute interval until a potential of about (−100 mV).

2.2. Tests for protective and non protective films

The film thickness was calculated by using (Gravimetric determination of film weight and thickness) according to the standard test method (ASTM B 680-80) (Frankel, 2004), from the weight loss measured in Equation (1). The specimens were weighed before immersion in the following chemical etching solution for mild steel (Uhlig, 2013): Hydrochloric acid 30 ml, ferrous chloride 10 g, deionized water 120 ml. The time for immersion is 10 min and the temperature of electrolyte is 25 °C. This solution does not attack mild steel but dissolves and cleans the thin corrosion products film (i.e., $FeCO_3$) and leaving the surface of mild steel. The specimen is weighed before and after film removal. The loss in weight divided by the area provides a figure for the mass of film per unit area (Marcus and Herbelin, 1993):

$$W_{Film} = \frac{W_f - W_{wf}}{A} \quad (1)$$

where: W_f = Weight of a specimen with the film in (g); W_{wf} = Weight of a specimen after film removal in (g); A = Surface area (dm^2). The density of a 100% $FeCO_3$ film is 3.96 g/cm^3 (Roberge, 2012). From the weight loss measured above, the film thickness can be calculated from Equation (2):

$$F_t = \frac{\left(W_f - W_{wf}\right) \times 10^4}{A \times \rho} \quad (2)$$

where: F_t = Film thickness in (micron). ρ = Density (g/cm^3).

A part from the appearance of the specimen after film removed, the completion of the stripping operation can be checked by repeating the immersion in chemical etching solution for another minute followed by drying and re-weighing. No further loss of weight shall occur. The specimens were rinsed in running water followed by distilled water to remove the excess solution, dried and weighed, the immersion in the above solution was repeating for another minutes followed by drying and re-weighing, no further loss in weight shall occur.

2.3. X-ray diffraction

To characterize and determine the phases of corrosion products present in the API X65 mild steel in presence and absence of acetic acid under the optimum conditions, X-ray diffraction studies were undertaken in (S.C. of Geological Survey and Mining) by using X-ray instrument type (Philips PW- 1840 (made in Holland)) X-ray diffractometer with the setting listed in Table 1. The X-ray examination was carried out to make sure that the entire surface was converted to scale film of corrosion products (iron carbide and ferrous carbonate) in presence and absence of acetic acid. In this work, ring shape specimen of API X65 mild steel with dimension 2.03 cm outside diameter, 2.08 cm width and 0.13 cm thickness. The peak of each element is aimed to describe the chemical compound formed of the corroded steel surface. Peak identification was made on the basis of d spacing of typical compounds given in the ASTM powder diffraction files of Ministry of Industry and Minerals-Baghdad.

2.4. Roughness test

Measuring the surface roughness of the protective mild steel film was carried out using (Taysurf – Taylor-Hobson Company-England) with the following specifications: Stylus material: Diamond, Stylus force: 100 mg.f. The arithmetic average values (Ra) for no protective and protective film formation specimens were calculated directly from the instrument. The examinations were carried out for API X65 mild steel with absence and presence of protective film formation specimens.

2.5. Hardness test

Vickers micro hardness (VMH) test was carried out for the specimens under optimum conditions for API X65 mild steel under no protective and protective film formation by using LARYEE Computerized Metallurgical Optical Microscopy Technique (W. Germany). The magnification was X100 and the applied load was 9.8 N. The average of 5 readings of the indentation length was taken while; the applied load was kept for 20 s for each reading. The Vickers micro-hardness (VMH) was computerized according to the following Equation:

Table 1
X-Ray diffractometer settings.

Scan Speed	5 deg/min
Wave Length	λ = 1.54060 Å
Current	30 mA
Voltage	40 kV

$$VMH = \frac{1.854 \times F}{D^2} \quad (3)$$

where: F is force (load) = 9.8 N, D is the diameter of measuring point in (μm).

2.6. Microstructure examination

The surface and cross-section microstructures evolution were characterized by using Scanning Electron Microscopy (SEM) and a Computerized Metallurgical Optical Microscopy Technique (CMOMT), (Type MeF$_2$), (Carllnsize Company – (Instruments Analytical, W. Germany, for analysis of the surface films)) with digital camera. The films were examined visually by optical microscopy under (5×) magnification power. These tests were achieved at the Ministry of Science and Technology-Baghdad. The specimens were prepared from API X65 mild steel before and also after corrosion in CO_2 saturated,3.5 wt% NaCl solution in presence and absence of acetic acid at the optimum conditions by the weight loss measurement (WL) for a period 3 h to observe the non-protective and protective film formation.

3. Results and discussion

The corrosion behavior of API X65 mild steel in CO_2 saturated, 3.5 wt% NaCl solution in presence and absence of acetic acid at different experimental conditions have been investigated by weight loss and polarization techniques as shown in Table 2.

3.1. Weight loss measurements

3.1.1. Experiments in a simulated brine solution

A series of weight loss technique experiments were performed in simulated brine of 3.5 wt% NaCl solutions saturated with CO_2 gas in presence and absence of acetic acid at different experimental conditions to study and verify the effect of the presence of multiple ions (Na^+, Cl^-, K^+, Ca^{+2}, Mg^{+2}) on the corrosion rates of API X65 mild steel. It was found that no significant difference can be seen from the weight loss measurements over three hours between the two solutions as shown in Fig. 1.

3.1.2. Absence of protective film

The corrosion rates of API X65 mild steel in 3.5 wt% NaCl saturated with CO_2 solutions in presence of different concentrations of acetic acid and different temperatures, pH's with speeds of rotation are summarized in Table 3 through 20 runs using weight loss technique. The field of variation of the 4 studied experimental factors was selected in order to approach the natural conditions which can be met in the experimental field. Classically, the various levels were expressed in a system of coded variables. Level +1 corresponded to the highest real value and level −1 to the lowest real value. The correspondence between real variables and coded ones was done starting from the following Equation:

$$x_i = \frac{X_i - X_i^0}{\Delta X_i}; \quad (i = 1, k) \quad (4)$$

where: x_i = value of the variable factor in i-coded; X_i = corresponding value of factor i in real variable; and X_i^0 = central value in the field of variation and k is the number of the input factors:

$$\Delta X_i = \text{variation pace} = \frac{X_i^{max} - X_i^{min}}{2}; \quad (i = 1, k) \quad (5)$$

Table 2
Different experimental conditions.

Variable	No protective film formation (presence of HAc)	Presence of protective film formation (absence of HAc)
Temperature (°C)	40, 50 & 60 °C	65, 70 & 75 °C
pH	3, 4 & 5	7.5, 8 & 8.5
HAc Acid Conc. (ppm)	1000, 2000 & 3000	–
Speed of Rotation (rpm)	1000, 1250 & 1500	1000, 1250 & 1500

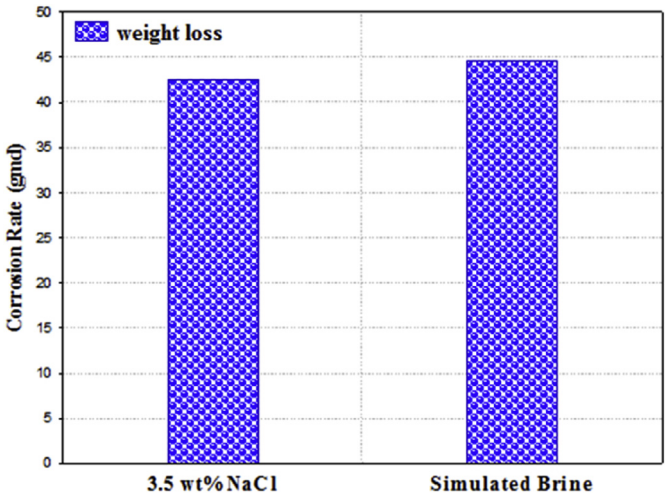

Fig. 1. The effect of 3.5 wt% NaCl and simulated brines solutions on the corrosion rate of API X65 mild steel in CO_2 saturated solutions (40 °C, pH 5, 3000 ppm HAc & 1000 rpm) by weight loss technique.

Table 3
Weight loss corrosion rates (gmd) results in presence of acetic acid (absence of protective film formation).

No.	T (°C)	pH	C_A (ppm)	ω (rpm)	W_1 (gm)	W_2 (gm)	C.R (gmd)
1.	40	3	1000	1000	25.4825	25.4744	48.52
2.	60	3	1000	1000	25.3988	25.3788	121.30
3.	40	5	1000	1000	25.1123	25.1057	40.06
4.	60	5	1000	1000	25.0431	25.0349	50.19
5.	40	3	3000	1000	24.7991	24.7907	51.22
6.	60	3	3000	1000	24.6995	24.6783	129.39
7.	40	5	3000	1000	24.7881	24.7811	42.53
8.	60	5	3000	1000	25.1199	25.1106	56.14
9.	40	3	1000	1500	24.2213	24.2127	52.65
10.	60	3	1000	1500	25.2182	25.1975	125.15
11.	40	5	1000	1500	24.3171	24.3099	43.67
12.	60	5	1000	1500	25.3915	25.3831	51.14
13.	40	3	3000	1500	24.6933	24.6841	55.69
14.	60	3	3000	1500	24.3487	24.3272	130.46
15.	40	5	3000	1500	24.7913	24.7837	46.02
16.	60	5	3000	1500	24.5321	24.5221	60.14
17.	50	4	2000	1250	25.3923	25.3817	63.81
18.	50	4	2000	1250	24.5318	24.5219	59.72
19.	50	4	2000	1250	24.7312	24.7208	62.43
20.	50	4	2000	1250	24.7110	24.7013	58.64

All fields of variation for the 4 studied factors are listed in Table 4. The experimental response of current study was the corrosion rate (gm/m^2.day); it is calculated by using the following Equation:

$$\text{Corr.Rate(gmd)} = \frac{(W_1 - W_2)}{A \times t} \quad (6)$$

where W_1 and W_2 are the weights of mild steel before and after test in grams, respectively, A is surface area in square meter and t is time in day. The response of experiments conducted according to four-factors, two-levels Full Factorial Experimental Design (FFED) (Box and Hunto, 2005). The results of experimental runs are shown in Table 5. This table shows the results of corrosion rates of the 20 experiments conducted at low (−1), center (0), and high (+1) levels of the studied variables. The selected design matrix was an FFED consisting of 20 rows of coded/real factors, corresponding to a number of trials. This design provides a uniform distribution of experimental points within the selected experimental hyper-space and the experiment with high resolution. Mathematical and Statistical Analysis were carried out. The linear, the quasi-linear, the quadratic, the power non-linear, exponential, and power mathematical models were selected for the analysis in this study. The parameters of equations have been estimated by means of the least-square method, using STATISTICA program software package® V.10. In this way, the following multiple regression equations in presence of acetic acid (absence of protective film formation) were obtained:

Table 5
Coded & real variables with the observed values of the response, (C.R) in presence of acetic acid (absence of protective film formation).

No.	Real factor				Coded factor				Response C.R (gmd)
	T	pH	C_A	ω	x_1	x_2	x_3	x_4	
1	40	3	1000	1000	−1	−1	−1	−1	48.52
2	60	3	1000	1000	+1	−1	−1	−1	121.30
3	40	5	1000	1000	−1	+1	−1	−1	40.06
4	60	5	1000	1000	+1	+1	−1	−1	50.19
5	40	3	3000	1000	−1	−1	+1	−1	51.22
6	60	3	3000	1000	+1	−1	+1	−1	129.39
7	40	5	3000	1000	−1	+1	+1	−1	42.53
8	60	5	3000	1000	+1	+1	+1	−1	56.14
9	40	3	1000	1500	−1	−1	−1	+1	52.65
10	60	3	1000	1500	+1	−1	−1	+1	125.15
11	40	5	1000	1500	−1	+1	−1	+1	43.67
12	60	5	1000	1500	+1	+1	−1	+1	51.14
13	40	3	3000	1500	−1	−1	+1	+1	55.69
14	60	3	3000	1500	+1	−1	+1	+1	130.46
15	40	5	3000	1500	−1	+1	+1	+1	46.02
16	60	5	3000	1500	+1	+1	+1	+1	60.14
17	50	4	2000	1250	0	0	0	0	63.81
18	50	4	2000	1250	0	0	0	0	59.72
19	50	4	2000	1250	0	0	0	0	62.43
20	50	4	2000	1250	0	0	0	0	58.64

Table 4
Center and variation step of parameters.

Factor		Unit	Centre	Variation step
X_1	Temperature	°C	50	10
X_2	pH		4	1
X_3	HAc Acid Concentration	ppm	2000	1000
X_4	Speed of Rotation	rpm	1250	250

Linear Model: R=0.877

$$\textbf{1)}\quad \hat{y} = 67.4436 + 21.4734\,x_1 - 20.2808\,x_2 + 2.4315\,x_3 + 1.5982\,x_4 \tag{7}$$

Quasi–Linear Model: R=0.994

$$\textbf{2)}\quad \hat{y} = 67.4436 + 21.4734\,x_1 - 20.2808\,x_2 + 2.4315\,x_3 + 1.5982\,x_4 - 15.8045\,x_1x_2 + 1.1114\,x_1x_3 - 0.3647\,x_1x_4 + 0.0406\,x_2x_3 - 0.0914\,x_2x_4 + 0.0309\,x_3x_4 \tag{8}$$

Quadratic Model: R=0.999

$$\textbf{3)}\quad \hat{y} = 61.1512 + 21.4734\,x_1 - 20.2808\,x_2 + 2.4315\,x_3 + 1.5982\,x_4 + 1.9664\,x_1^2 + 1.9664\,x_2^2 + 1.9664\,x_3^2 + 1.9664\,x_4^2 - 15.8045\,x_1x_2 + 1.1114\,x_1x_3 - 0.3647\,x_1x_4 + 0.0406\,x_2x_3 - 0.0914\,x_2x_4 + 0.0309\,x_3x_4 \tag{9}$$

Multiple Power Model: R=0.966

$$\textbf{4)}\quad \hat{y} = 311.4988 + 18.1122\,x_1 - 1.3642\,x_2 + 60.233\,x_3 + 21.6193\,x_4 \tag{10}$$

Exponential & *Multiple Power Model*: R=0.965

$$\textbf{5)}\quad \hat{y} = 343.1143 - 20.2615x_1 - 1.3730x_2 + 69.5x_3 + 40.7x_4 \tag{11}$$

The coding of the process factors was carried out according to the Equation:

$$x_i = \frac{X_i - X_i^0}{\Delta X_i}; \quad (i = 1, k) \tag{12}$$

where x_i, i = 1, 2, 3 &4 are in their coded levels ranged (−1, 0, +1), this equation is applied to setup the relationship between the coded level and the corresponding real variables. The fitted multiple regression Equations in terms of the real levels of the solution temperature, the pH, the HAc acid concentration and the speed of rotation may be obtained by substituting the transforming Equation (12) into the Equations 7–11 as follows:

$$x_1 = \frac{X_1}{10} - 5, \quad x_2 = X_2 - 4$$

$$x_3 = \frac{X_3}{1000} - 2, \quad x_4 = \frac{X_4}{250} - 5$$

From the regression Equation (the quadratic model) the optimized values are calculated by partial differentiating the above Equation with respect to x_1, x_2, x_3 & x_4 and equating to zero solving the four Equations from partial differentiation results in the optimal corrosion rate. The final optimal conditions are:

Variable	Code	Real
Temperature, °C	−0.5	45.4
pH	0.8	4.8
HAc Acid Conc., ppm	0.2	2178.5
Speed of Rotation, rpm	0.2	1296.6

To determine the significance of the above mentioned effect, an analysis of variance (ANOVA) was carried out. The corresponding analysis of variance is represented in Table 6. The new response function is then written in the following form:

$$\hat{y} = 61.1512 + 21.4734\,x_1 - 20.2808\,x_2 + 2.4315\,x_3 + 1.5982\,x_4 + 1.9664\,x_1^2 + 1.9664\,x_2^2 + 1.9664\,x_3^2 + 1.9664\,x_4^2 - 15.8045\,x_1x_2 \tag{13}$$

The preliminary information of the quantitative and qualitative impact on the objective function (response) of each individual factor in the regression Equations can be obtained from its parameters sign and magnitude (Jeff Wu and Michael, 2009). The positive sign for the parameters of the temperature of solution, the HAc acid concentration and the speed of rotation indicates that the corrosion rate increases (response surface deteriorates) with the increase in these three factors. The negative sign for the parameter of the solution pH shows that the corrosion rate decreases (response surface improves) with the increase in the solution pH. Furthermore, the given quadratic regression equation and Pareto chart as shown in Fig. 2 suggests that the dominant process factor is the temperature of solution, while the effects of the solution pH, the HAc acid concentration and the speed of rotation are considerably smaller. The factor interactions and quadratic (square) have generally the least influence on the considered problem, except the factor interaction between the temperature and the solution pH. In order to take into account the contribution from the remainder factor interactions, these terms were not neglected.

3.1.3. *Presence of protective film*

Similar calculations were also done in absence of acetic acid at different temperatures, pH's, and speeds of rotation. Table 7 through 12 runs using weight loss technique. Again the quadratic model was the most accurate mathematical equation (0.999 of correlation coefficient) with following optimal conditions:

Variable	Code	Real
Temperature, °C	−0.3	68.7
pH	−0.2	7.9
Speed of Rotation, rpm	0.7	1425.8

ANOVA and statistical analysis yield the following significant equation:

$$\hat{y} = 19.0775 + 8.9932\,x_1 - 1.9540\,x_2 + 1.3881\,x_3 + 2.0725\,x_1^2 + 2.0725\,x_2^2 + 2.0725\,x_3^2 \tag{14}$$

The positive sign for the parameters of the temperature of solution and the speed of rotation indicates that the corrosion rate increases with the increase in these two factors. The negative sign for the parameter of the solution pH shows that the corrosion rate decreases with the increase in the solution pH.

3.2. *Effect of environmental parameters*

3.2.1. *Effect of temperature*

As shown in Fig. 3, the corrosion rate increased with temperature in presence and absence of protective film. Activation parameters for some systems can be estimated either from an Arrhenius-type plot (Eq. (15)) or from transition state theory (Eq. (16)).

Table 6
Analysis of variance (ANOVA) for API X65 mild steel alloy corrosion in absence of protective film formation.

Constant estimated	Source	$\sum x^2$	Estimate coefficient (b)	Variance $S_b^2 = S_r^2/\sum x^2$	F-value $= b^2/S_b^2$	$F_{0.95(1,5)} = 6.61$
b_1	Linear	16	21.4734	0.2735	1685.9485	S
b_2		16	−20.2808	0.2735	1503.8788	S
b_3		16	2.4315	0.2735	21.6168	S
b_4		16	1.5982	0.2735	9.3391	S
b_{11}	Square	16	1.9664	0.2735	14.1379	S
b_{22}		16	1.9664	0.2735	14.1379	S
b_{33}		16	1.9664	0.2735	14.1379	S
b_{44}		16	1.9664	0.2735	14.1379	S
b_{12}	Interaction	16	−15.8045	0.2735	913.2805	S
b_{13}		16	1.1114	0.2735	4.5163	NS
b_{14}		16	−0.3647	0.2735	0.4863	NS
b_{23}		16	0.0406	0.2735	0.0060	NS
b_{24}		16	−0.0914	0.2735	0.0305	NS
b_{34}		16	0.0309	0.2735	0.0035	NS

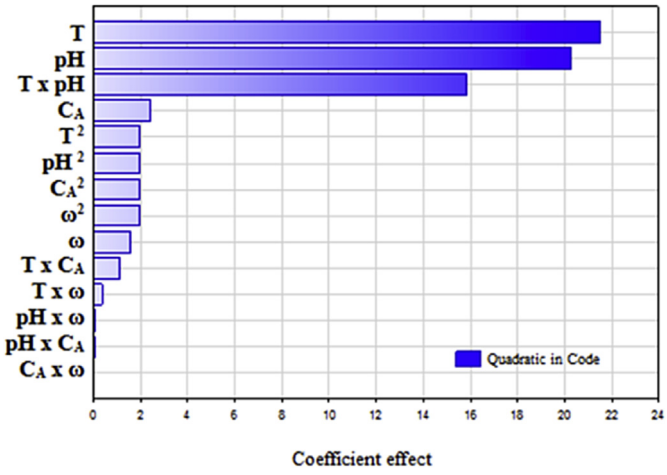

Fig. 2. Pareto chart for API X65 mild steel in presence of acetic acid (absence of protective film formation).

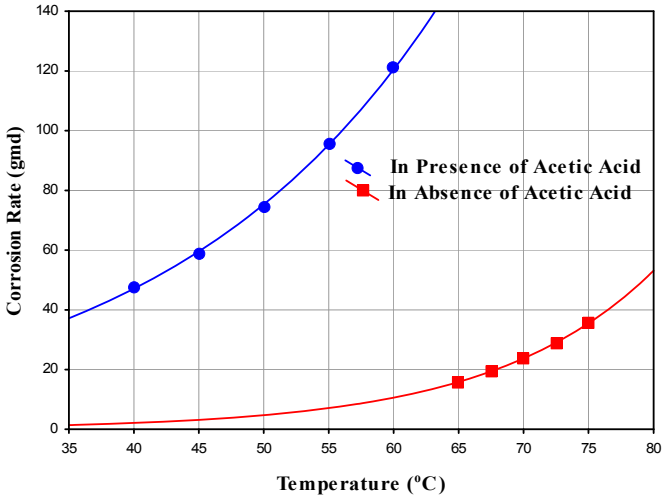

Fig. 3. The Variation of Corrosion Rate with Temperature of API X65 Mild Steel in CO_2 Saturated, 3.5 wt% NaCl Solution at (pH 3, 1000 ppm HAc and 1000 rpm) and (pH 7.5 and 1000 rpm).

Table 7
Weight loss corrosion rates (gmd) results in absence of acetic acid (presence of protective film formation).

No.	T (°C)	pH	Ω (rpm)	W_1 (g)	W_2 (g)	C.R (gmd)
1.	65	7.5	1000	25.2763	25.2737	15.88
2.	75	7.5	1000	24.6846	24.6788	35.49
3.	65	8.5	1000	24.6801	24.6781	12.44
4.	75	8.5	1000	24.5746	24.5694	31.82
5.	65	7.5	1500	24.1130	24.1097	20.53
6.	75	7.5	1500	25.5203	25.5143	37.09
7.	65	8.5	1500	25.2609	25.2582	16.35
8.	75	8.5	1500	25.0484	25.0431	32.76
9.	70	8	1250	24.8659	24.8628	19.17
10.	70	8	1250	24.5417	24.5386	19.20
11.	70	8	1250	24.5678	24.5647	18.99
12.	70	8	1250	24.4456	24.4425	18.95

$$k = A\,Exp\left(-\frac{E}{RT}\right) \quad 15$$

$$k = \left(\frac{RT}{Nh}\right)exp\left(-\frac{\Delta H^*}{RT}\right)exp\left(\frac{\Delta S^*}{R}\right) \quad 16$$

where K is Reaction rate, A is Modified frequency factor (pre-exponential factor), E is Activation energy (J mol^{-1}), R is Gas constant (8.314 J mol^{-1} K), T is Absolute temperature (K), ΔH^* is Enthalpy of activation, ΔS^* is Entropy of activation, N is Avogadr's number (6.022×10^{23} molecule mol^{-1}), h is Plank's constant (6.626×10^{-34} J s mol^{-1}). These equations can be linearized and drawn, slopes and intercepts produce the values of activation parameters (Figs. 4 and 5). It is observed that in presence of acetic acid, generally, the values of E_a, ΔH^* and ΔG are smaller than the values obtained in absence of the acetic acid, but the values of K^* are larger than the values obtained in absence of the acetic acid as shown in Table 8. This can be, attributed, to the formation of the protective film on the metal surfaces that; the reaction needs more energy to take place. The results showed positive values for both activation energy E_a and activation enthalpy ΔH^* reflecting the endothermic nature of the corrosion process. The same behavior observed with the values of ΔS^*, the values are also negative in absence of the acetic acid at speeds of rotation (1000 and 1500 rpm), and it increased with increasing in pH values of the solution. The negative values of activation entropy ΔS^* pointed to greater order being produced during the activation process. This can be achieved by the formation of the activated complex represented by the film formation. (Aprael et al., 2011). In presence of the acetic acid at different conditions the Transition State of the rate – determining recombination step represents a more orderly arrangement relative to the initial state, and hence, a negative values for ΔS^* is obtained.

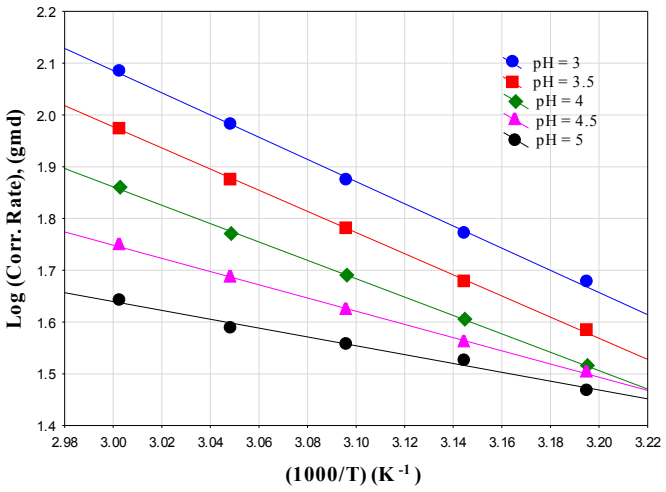

Fig. 4. Arrhenius Plot for API X65 Mild Steel in CO_2 Saturated, 3.5 wt% NaCl Solutions in Presence of Acetic Acid and without Protective Film Formation at 1000 ppm HAc & 1000 rpm.

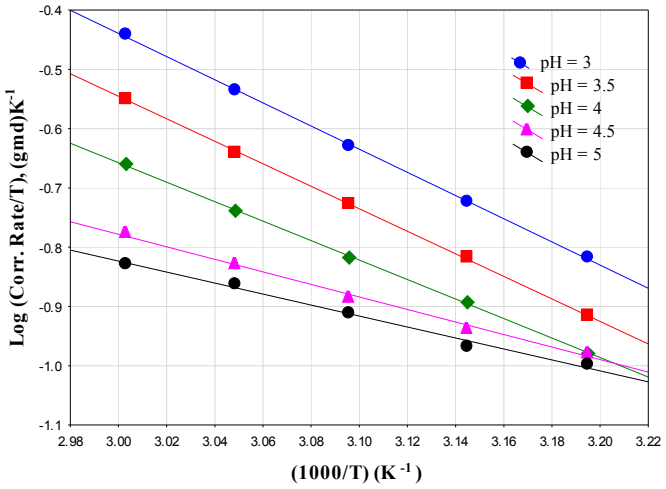

Fig. 5. Transition State Equation Plot for API X65 Mild Steel in CO_2 Saturated, 3.5 wt% NaCl Solutions in Presence of Acetic Acid and without Protective Film Formation at 1000 ppm HAc & 1000 rpm.

3.2.2. Effect of pH

Fig. 6 shows the relationship between corrosion rates and pH at given temperatures at optimum conditions, in presence and absence of acetic acid. In presence of acetic acid, the analysis of the response function (corrosion rate) showed that pH is slightly less pronounced than the temperature. The corrosion rate decreased as the pH value increased until it reaches pH 4.8 at 45 °C then slightly increased as the pH value increased. This behavior can be attributed to the formation of corrosion products scales (Fe_3C + $FeCO_3$). Increasing the pH from 3 to 4.8 at 45 °C gives an increase in the formation products scale layer greater than the increase in the dissolution of metal which increased the anodic reaction (Uhlig and Winston, 2008). On the contrary, increasing the pH value up to pH 4.8 gave a negative net represented by the decrease in the formation of a very porous and non-protective film thickness and slightly increases in the corrosion rate. In absence of acetic acid, the analysis of the response function showed that pH is less pronounced than the temperature on the corrosion rate, but showed that the interaction is the factor which has the lowest effect on the corrosion rate. It can be seen that the corrosion rate slightly increases as the pH value increases until it reaches pH 7.9 at 68 °C then decreases as the pH value increases. This behavior can be attributed to increasing activity of H^+ ions, indirectly accelerated corrosion kinetics (Jiabin et al., 2011) and the corrosion rate increases therefore the dissolution rate of metal which increases the anodic reaction (Uhlig and Winston, 2008). On the other hand further increase in pH value results in the increase of the formation (deposition) rate of protective film thickness and covering (inhibiting) a portion of the steel surface due to protective film formation is accelerated by measures that restrict the transport of reaction products from the surface (Dugstad et al., 2000) and decrease in the corrosion rate. Also, it is clear that, increasing the pH from 7.5 to 7.9 at 68 °C gave an increase in the dissolution of metal which increased the anodic reaction (Uhlig and Winston, 2008) greater than the increase in the formation rate of corrosion product film therefore the positive net from these two factors represented by the increase in the corrosion rate. On the contrary, increasing the pH value up to pH 7.9 gave a negative net represented by the increase in the formation of a dense protective film thickness and decrease in the corrosion rate.

3.2.3. Effect of acetic acid concentration

Fig. 7 represents the effect of acetic acid concentration on the corrosion rate. Corrosion rate increased as the acetic acid concentration increased until it reaches 2178.5 ppm at 45 °C then decreased as the acetic acid concentration increased. This behavior can be attributed to: The significant increase of corrosion rate is due to the increase in cathodic reaction. As reported by Tran et al. (Tran et al., 2013). HAc increases cathodic reaction by dissociation of acetic acid and direct reduction of undissociated HAc molecules. Also, this is due to the degradation of non-protective film by HAc, since acetate ions have the ability to form iron acetate and transport iron away from the steel surface (Zhang and Cheng, 2009) then the corrosion rate decreased by non-protective film formation (i.e., these films can significantly alter the corrosion process by either decreasing the corrosion rate by acting as a diffusion barrier, or increasing the corrosion (Gulbrandsen et al., 1998) by increasing the active specimen surface area) is accelerated by measures that restrict the transport of reaction products from the surface (Tran et al., 2013). Furthermore, an investigation shows that the corrosion rate rises at higher temperatures and HAc concentrations. This is due to acceleration of anodic and cathodic reactions when the temperature increases (George and Nesic, 2007; George, 2003). The increase of cathodic reaction in CO_2 corrosion is due to the HAc contribution to hydrogen ions through possibly dissociation and reduction. It is worthwhile to note that below the inhibitive level, the higher the concentration of acetic acid, the higher is the number of hydrogen ions produced. At higher temperature, the diffusion coefficient of HAc is higher, which results in more available species, approximately a twofold increase in the corrosion rate with 2000 ppm HAc at 60 °C than at 40 °C. At 40 °C, the value of the diffusion coefficient of HAc is 1.6×10^{-9} m^2/s, whereas at 60 °C it is 2.3×10^{-9} m^2/s, which is 85% higher. It is clear that, increasing the concentration of acetic acid from 1000 to 2178.5 ppm at 45 °C gave an increase in the corrosion rate of metal surface greater than the increase in the formation rate of corrosion scale film, therefore the positive net from these two factors represented by the increase in the corrosion rate. On the contrary, increasing the concentration of acetic acid up to 2178.5 ppm gave a negative net represented by the decrease in the corrosion rate by non-protective film formation by acting as a diffusion barrier (Gulbrandsen et al., 1998) and accelerated by measures that restrict the transport of reaction products from the surface (Dugstad et al., 2000). A different corrosion rate trend is observed with the presence of HAc at range (1000–3000 ppm) under turbulent conditions at different temperatures. The corrosion rate increases with increasing HAc

Table 8
Activation Parameters for the Corrosion Process of API X65 Mild Steel in CO_2 Saturated, 3.5 wt% NaCl Solution in Presence and Absence of Acetic Acid at Different Conditions.

Temp. Range (°C)	pH	HAc conc. (ppm)	Speed of rotation (rpm)	ΔS^* (kJ/K.mol.)	ΔH^* (kJ/mol.)	E_a (kJ/mol.)	Average ΔG (kJ/mol.)	Average K^* equlibrium constant
40–60	3	1000	1000	−0.205	37.42	41.01	103.635	1.8E-17
40–60	3.5	1000	1000	−0.207	36.36	39.09	103.221	2.1E-17
40–60	4	1000	1000	−0.209	31.49	33.99	98.997	1.0E-16
40–60	4.5	1000	1000	−0.212	20.23	24.43	88.706	4.6E-15
40–60	5	1000	1000	−0.213	17.73	16.37	86.529	1.0E-14
40–60	3	3000	1000	−0.205	36.95	39.76	103.165	2.2E-17
40–60	3.5	3000	1000	−0.207	35.79	39.96	102.651	2.6E-17
40–60	4	3000	1000	−0.209	31.01	33.97	98.517	1.2E-16
40–60	4.5	3000	1000	−0.211	22.88	25.39	91.033	1.9E-15
40–60	5	3000	1000	−0.212	20.65	23.58	89.126	3.9E-15
40–60	3	1000	1500	−0.205	35.09	28.11	101.305	4.3E-17
40–60	3.5	1000	1500	−0.207	33.49	36.02	100.351	6.1E-17
40–60	4	1000	1500	−0.209	28.43	30.96	95.937	3.1E-16
40–60	4.5	1000	1500	−0.212	18.79	21.53	87.266	7.8E-15
40–60	5	1000	1500	−0.213	15.93	19.20	84.729	1.9E-14
40–60	3	3000	1500	−0.205	34.77	38.18	100.985	4.8E-17
40–60	3.5	3000	1500	−0.206	33.29	35.98	99.828	7.3E-17
40–60	4	3000	1500	−0.209	28.74	31.07	96.247	2.8E-16
40–60	4.5	3000	1500	−0.211	19.59	23.22	87.743	6.5E-15
40–60	5	3000	1500	−0.212	16.29	21.79	84.766	1.9E-14
65–75	7.5	Blank Solution	1000	−0.219	90.09	93.28	165.207	7.3E-26
65–75	7.75	Blank Solution	1000	−0.218	65.54	71.42	140.314	4.4E-22
65–75	8	Blank Solution	1000	−0.217	60.34	63.50	134.771	3.1E-21
65–75	8.25	Blank Solution	1000	−0.218	72.04	74.68	146.814	4.5E-23
65–75	8.5	Blank Solution	1000	−0.221	112.88	115.19	188.683	2.0E-29
65–75	7.5	Blank Solution	1500	−0.219	62.77	66.01	137.887	1.0E-21
65–75	7.75	Blank Solution	1500	−0.217	49.28	52.37	123.711	1.5E-19
65–75	8	Blank Solution	1500	−0.217	47.39	49.44	121.478	3.2E-19
65–75	8.25	Blank Solution	1500	−0.218	53.43	56.39	128.204	3.0E-20
65–75	8.5	Blank Solution	1500	−0.221	78.00	82.61	153.803	3.9E-24

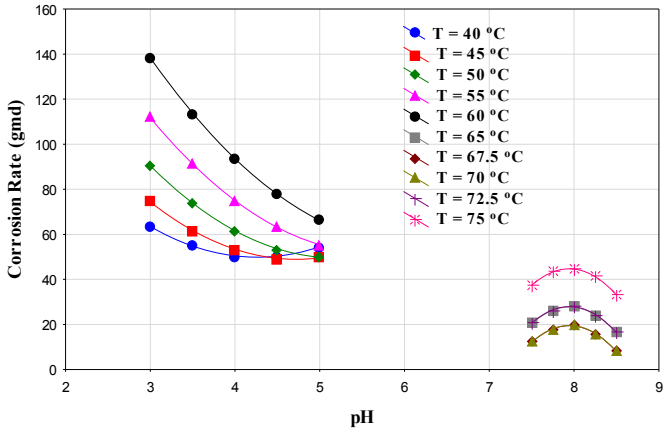

Fig. 6. The Effect of pH on the Corrosion of API X65 Mild Steel in CO_2 saturated, 3.5 wt% NaCl Solution in Presence and Absence of Acetic Acid (Absence and Presence of the Protective Film Formation) at (2178.5 ppm HAc and 1296.6 rpm) and (1425.8 rpm).

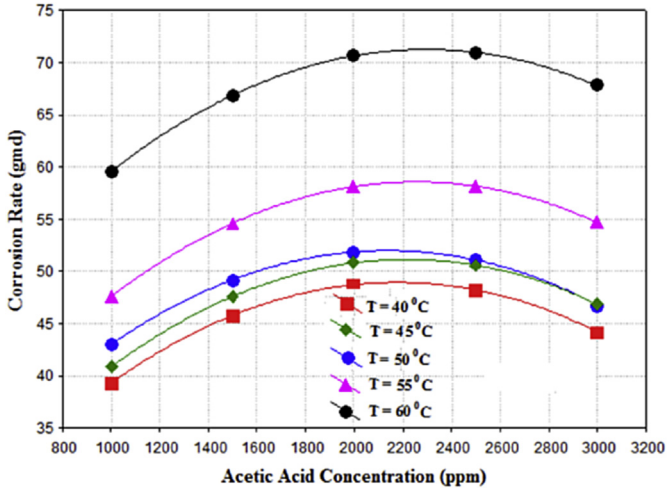

Fig. 7. The Effect of Acetic Acid Concentration on the Corrosion of API X65 Mild Steel in CO_2 saturated, 3.5 wt% NaCl Solution in Presence of Acetic Acid (Absence of the Protective Film Formation) at (pH 4.8 and 1296.6 rpm).

concentration. However, at 45 °C and pH 4.8, the corrosion rate decreases with more than 2178.5 ppm HAc. Furthermore, it is worth noting that an appreciable effect of HAc at 45 °C and pH 4.8 was only observed beyond 2178.5 ppm HAc, which recorded an approximately 12% increase in the corrosion rate. Fig. 7 shows that increase of HAc concentration and temperature leads to an increase of corrosion rate. In the range of experiments, at optimum temperature 45 °C have increased corrosion rate to 48.9 gmd. This increase the corrosion rate as an effect of HAc concentration and temperature was also observed by Mokhtar (Mokhtar, 2005) and James (James, 2004) and George and Nesic (Jeff Wu and Michael, 2009). They all agreed with the role of ions activities that took part in contributing on corrosion rate.

3.2.4. Effect of speed of rotation

Fig. 8 shows the effect of speed of rotation on corrosion rate of mild steel in absence and presence of the protective film at different temperatures at optimum conditions. In absence of the protective film, it is clear that the speed of rotation is less pronounced than the temperature on the corrosion rate, but showed that the interaction is the factor which has the lowest effect on the corrosion rate. It can be seen that the corrosion rate increased as the speed of rotation increased until it reaches 1296 rpm at 45 °C then decreased as the speed of rotation increased. This behavior can be attributed to: When the speed of rotation increased, the corrosion rate increased and resulted in an enhanced value of the corrosion rate on pure

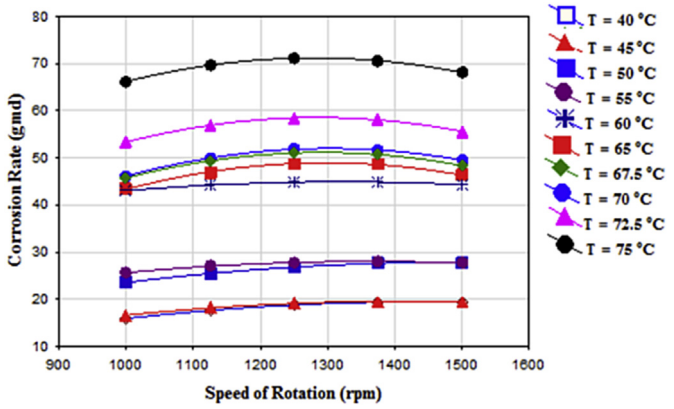

Fig. 8. The Effect of Speed of Rotation on the Corrosion of API X65 Mild Steel in CO_2 saturated, 3.5 wt% NaCl Solution in Presence and Absence of Acetic Acid (Absence and Presence of the Protective Film Formation) at (pH 4.8 and 2178.5 ppm HAc) and (pH 7.9).

kinetic ground because of the speed of rotation lead to removal any layers, corrosion products or deposits from the surface and get a more active surface (i.e., the formation rate of corrosion products scale ($Fe_3C + FeCO_3$) non protective film decreased). On the other hand further increase in speed of rotation results in the increase of the formation rate of corrosion products on the metal surface and decrease corrosion rate because for a not fully developed protective film surface, the effect of speed of rotation is related to the transport of species towards and away from the metal surface. It is clear that, increasing the speed of rotation from 1000 to 1296 rpm at 45 °C gave an increase in the dissolution of metal which increases the anodic reaction (Nesic, 2007) greater than the increase in the formation rate of corrosion scale therefore the positive net from these two factors represented by the increase in the corrosion rate. On the contrary, increasing the speed of rotation up to 1296 rpm gave a negative net represented by the decrease in the corrosion rate. In presence of the protective film formation, the speed of rotation is less pronounced than the temperature on the corrosion rate, but showed that the interaction is the factor which has the highest effect on the corrosion rate. It can be seen that the corrosion rate increased as the speed of rotation increased until it reaches 1425 rpm at 68 °C then slightly decreased as the speed of rotation increased. This behavior can be attributed to: When the speed of rotation increased, the corrosion rate increased because the formation rate of corrosion products scale ($FeCO_3$) protective film thickness decreased. On the other hand further increase in speed of rotation results in the increase of the formation rate of protective film thickness and decrease corrosion rate. Increasing the speed of rotation from 1000 to 1425 rpm at 68 °C gave an increase in the dissolution of metal which increased the anodic reaction (Nesic, 2007) greater than the increase in the formation rate of corrosion scale therefore the positive net from these two factors represented by the increase in the corrosion rate. On the contrary, increasing the speed of rotation up to 1425 rpm gave a negative net represented by the decrease in the corrosion rate by protective film formation is accelerated by measures that restrict the transport of reaction products from the surface (Dugstad et al., 2000). It can be seen that the protective film thickness decreased and corrosion rate increased as the speed of rotation increased until it reaches 1425 rpm which is consistent with Faraday's law then film thickness increased as the speed of rotation increased. This behavior can be attributed to: When the speed of rotation increased, the dissolution of metal which increased the anodic reaction (Uhlig and Winston, 2008), because the protective film formation process on steel surface include three essential stages where these need to accelerate corrosion, during these stages can show speed of rotation influence on protective film thickness, essential stages for protective layer formation include (Nesic, 2007):

a. Attacked stage of corrosive solution to the steel surface and accumulation of layers of insoluble corrosion products on the steel surface.
b. Formation stage of a diffusion barrier for the species involved in corrosion process.
c. Formation stage of protective layer (dense layer).

At speed of rotation 1425 rpm the dissolution rate of metal surface is equal to the formation rate of the protective film. Thus the mathematical optimum speed of rotation is equal to 1425 rpm.

3.3. Electrochemical measurements

3.3.1. Open circuit potential (OCP)

The values of OCP were measured from the experimental runs. The steady state potentials were reached within one hour. Table 9 summarizes the values of OCP at different conditions. The measure OCP are found very close to the values given in the literature Zhang and Cheng (Zhang and Cheng, 2009) and Tran et al. (Tran et al., 2013). In presence of 1000 ppm & 3000 ppm acetic acid at pH 3 & pH 5 respectively, the OCP potential shifts to more negative (more active) direction as the temperature increased from 40 to 60 °C associated with speed of rotation increases from 1000 to 1500 rpm. The same behavior observed in absence of acetic acid at pH's (7.5 and 8.5), the increasing in temperature and speed of rotation lead to shift the OCP potential to more negative (active) values. But the OCP in absence of HAc are more positive in comparison with in presence of acetic acid. This shift towards higher anodic potential can be explained by the possible formation of an iron carbonate film and by the effect of temperature, pH and speed of rotation on the cathodic diffusion current. There is occasionally a change in Tafel slopes of polarization curve, more usually the cathodic one, possibly because of alteration of structure of double layer attendant upon protective film formation and hence changes in α (i.e. symmetry coefficient) (Bagotsky, 2006). The recorded open circuit potential values were close to those measured by Zhang and Cheng (Zhang and Cheng, 2009) and Tran et al. (Tran et al., 2013) at nearly similar test conditions (Fig. 9).

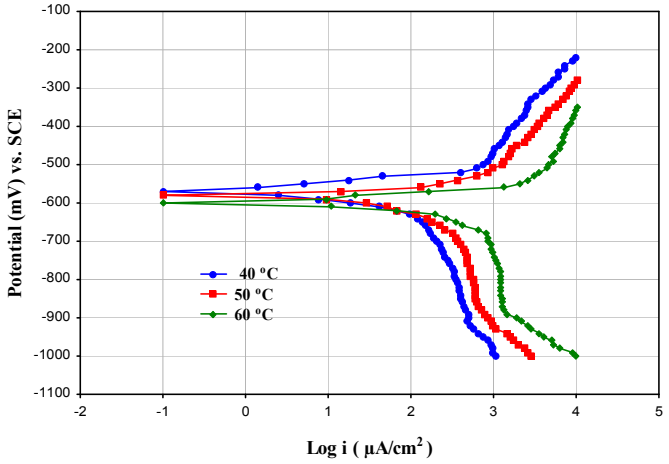

Fig. 9. Polarization Curves for the Corrosion of API X65 Mild Steel in CO_2 saturated,3.5 wt % NaCl in Presence of Acetic Acid at pH 3, 1000 ppm HAc and Speed of Rotation 1000 rpm.

Table 9
Open circuit potential values in presence and absence of acetic acid at different conditions.

Run No.	Temp. (°C)	pH	HAc conc. (ppm)	Speed of rotation (rpm)	OCP (mV),SCE
1	40	3	1000	1000	−560
2	50				−565
3	60				−585
4	40	3	1000	1250	−573
5	50				−582
6	60				−600
7	40	3	1000	1500	−597
8	50				−604
9	60				−613
10	40	5	3000	1000	−523
11	50				−529
12	60				−548
13	40	5	3000	1250	−529
14	50				−548
15	60				−567
16	40	5	3000	1500	−559
17	50				−560
18	60				−568
19	65	7.5	Blank Solution	1000	−412
20	70				−435.5
21	75				−465
22	65	7.5	Blank Solution	1250	−414
23	70				−439
24	75				−471
25	65	7.5	Blank Solution	1500	−422
26	70				−447.5
27	75				−481
28	65	8.5	Blank Solution	1000	−345
29	70				−398
30	75				−408
31	65	8.5	Blank Solution	1250	−406
32	70				−429
33	75				−444
34	65	8.5	Blank Solution	1500	−413
35	70				−440
36	75				−446

3.3.2. *Potentiodynamic polarization curves*

The corrosion behavior of API X65 mild steel in CO_2 saturated, NaCl solution in presence and absence of acetic acid was studied using polarization measurements. A total of 36 runs were carried out at different conditions. In absence of protective film, Fig. 10 showed the polarization curves obtained for API X65 in CO_2 saturated, NaCl solution, at different temperatures and speeds of rotation. A similar behavior is observed for the whole range of temperatures at all speeds of rotation and acetic acid concentrations. A plateau corresponding to a limiting current density (i_{lim}) is observed in the cathodic region of the polarization curves between (−1000, −700 mV SCE) at pH = 3. Therefore the cathodic reaction seems to be controlled by diffusion. Similar behavior can be seen at pH = 5, but the plateau corresponding to ($i_{lim.}$) current density is not so clear compared with pH = 3. With regard to the anodic branch of the polarization curves, anodic current density continuously increases as potential shifts to more positive values, not reaching stability. This fact means that the API X65 mild steel experiencing a corrosion process and it cannot reach a passivation state. Fig. 10 shows the polarization curves in presence of protective film formation, at different temperatures, solution pH values, and speeds of rotation. In this case the cathodic region of the polarization curves, and the cathodic reactions occurred seems to be activation complicated by diffusion (mass transfer), leading to disappearance of the plateau corresponding to a limiting current density. With regards to the anodic branch of the polarization curves. Similar behavior as in absence of protective film can be seen clearly. (i.e., the higher the potential shift to the positive direction, the higher the anodic current density leading to no passivity state reaching). The corrosion current densities and corrosion potentials were estimated by Tafel extrapolation of cathodic and anodic curves to the corrosion potentials. The Tafel slopes were estimated as well. Table 10 shows the corrosion current densities, corrosion potentials, and cathodic/anodic Tafel slopes at different experimental conditions. In all cases the extrapolation started over about 50 mV away from E_{corr}, and the same range of potential values has been always used. Therefore it has been considered that the obtained i_{corr} values are accurate enough to study the influence of

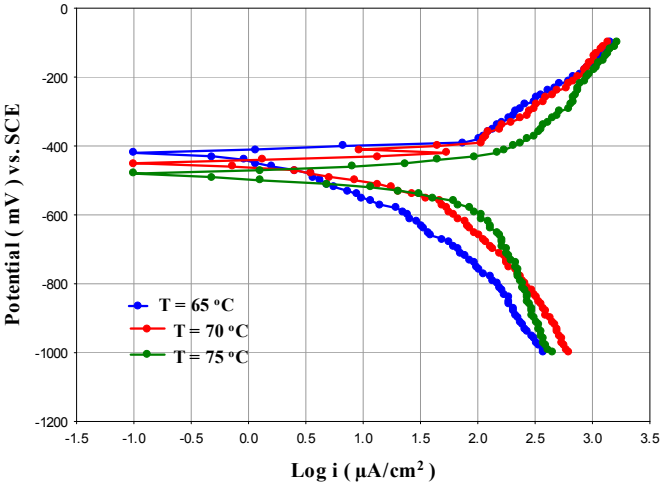

Fig. 10. Polarization Curves for the Corrosion of API X65 Mild Steel in CO_2 saturated, 3.5 wt % NaCl in Absence of Acetic Acid at pH 7.5 and Speed of Rotation 1000 rpm.

temperature, pH, acetic acid concentration, and speed of rotation on corrosion process. The polarization curves provide information about effects of changes in potential on the corrosion of the cathode as current density (current per unit area). Since the electrolyte is seawater (salt water), the concentration polarization type is predominant (Jezmar, 2002). From polarization curves, it can be determined practically the free corrosion potential, E_{corr} and limiting current density, $i_{lim.}$. Where E_{corr} is determined when the potential becomes approximately constant with decreasing current density. The limiting current plateau is not well defined, thus the method given by Gabe and Makanjoula (Gabe and Makanjoula, 1986) will be adopted to find i_{lim} values:

$$i_{lim} = \frac{i_1 + i_2}{2} \tag{17}$$

where, i_1 and i_2 are the current associated with E_1 and E_2 respectively. The values of corrosion current density increase with increasing in temperatures and speeds of rotation in both the presence and absence of acetic acid (i.e., absence and presence of the protective film formation) at different experimental conditions. But the corrosion current densities in absence of HAc are small in comparison with in presence of acetic acid. Temperature increases the rate of almost all chemical reactions (Shrier et al., 2000) and Uhlig (Uhlig, 2011). Therefore the effect of temperatures is to increase the anodic and cathodic current in presence and absence of acetic acid for a given pH value. Values of E_{corr} shift to more negative (more active) direction with increasing in temperatures and speeds of rotation in both the presence and absence of acetic acid at different experimental conditions. Corrosion potentials in absence of HAc are more positive in comparison with in presence of acetic acid. Nervana (Nervana, 2010) pointed out that the main effect of increasing the temperature is to increase the exchange current, when the process is under activation control. George and Nesic (George and Nesic, 2007) and Hernandez et al. (Hernandez et al., 2012) presented the analysis of activation controlled cathodic reaction complicated by mass transport effect and discussed its influence on corrosion parameters. In both presence and absence of acetic acid, the values of limiting diffusion current density were increased with both temperature and speed of rotation increasing. The limiting diffusion current densities in absence of HAc are lower in comparison with in presence of acetic acid. The calculated values of the anodic Tafel slopes, b_a in presence and absence of acetic acid at different experimental conditions, are shown as a function of the temperature, pH, HAc acid concentration, and speed of rotation of the electrode. As can be observed, in general terms, as the speed of rotation increases, the measured b_a remains relatively constant. This provides experimental evidence on the charge-transfer control of the anodic reaction, and therefore a mechanism that is not affected by speed of rotation. The values of the calculated cathodic Tafel slopes b_c, in this region are dependent on the data range considered. However, they are found to fall between −221 and −598 mV shown in Table 10. The variance in cathodic Tafel slopes in absence and presence of the protective film formation may be ascribed to changes in the symmetry of the energy barrier (α departs from 0.5) and the temperature (Bagotsky, 2006). In general, in presence of the protective film formation at pH 8.5 and different speeds of rotation (1000, 1250 and 1500 rpm), the values of b_c and b_a were approximately unchanged compared

Table 10
Corrosion parameters obtained (by Tafel extrapolation method) from polarization curves at different conditions.

Run No.	Temp. (°C)	pH	HAc conc. (ppm)	Speed of rotation (rpm)	b_a (mV)	$-b_c$ (mV)	i_{corr} (μA/cm^2)	E_{corr} (mV,SCE)	i_{lim} (μA/cm^2)
1	40	3	1000	1000	123.9	347.3	200.96	−572	251.77
2	50				141.1	421.4	255.76	−580	290.38
3	60				154.6	575.3	495.43	−600	601.91
4	40	3	1000	1250	136.9	348.4	233.91	−582	563.74
5	50				148.8	435	292.58	−596	1124.79
6	60				152.8	550	552.56	−616	2324.18
7	40	3	1000	1500	137.5	349	257.49	−610	706.37
8	50				148.9	428	354.36	−620	1365.88
9	60				150.5	595	570.28	−628	2391.48
10	40	5	3000	1000	138.5	334	176.97	−536	485.05
11	50				148.6	425	185.51	−544	538.84
12	60				159.4	580	214.99	−563	787.12
13	40	5	3000	1250	135.9	338	177.14	−545	437.63
14	50				148.7	475	197.61	−562	565.66
15	60				152.0	598	233.36	−576	1807.69
16	40	5	3000	1500	136.9	343	190.95	−570	549.59
17	50				148.8	433	215.03	−575	823.92
18	60				151.0	578	231.01	−580	2271.21
19	65	7.5	Blank Solution	1000	91.8	285	70.30	−423	186.96
20	70				82.7	393	98.03	−451.5	224.52
21	75				73.4	415	132.3	−480	282.38
22	65	7.5	Blank Solution	1250	91.3	227	76.50	−427	204.59
23	70				82.4	325	110.57	−456	235.15
24	75				73.2	444	134.44	−485	256.48
25	65	7.5	Blank Solution	1500	91.5	237	88.92	−430	172.53
26	70				79.3	308	123.03	−462.5	224.67
27	75				67.2	424	138.71	−495	297.72
28	65	8.5	Blank Solution	1000	95.3	221	56.51	−353	163.58
29	70				85.1	320	96.27	−412	226.52
30	75				73.3	439	117.60	−425	297.18
31	65	8.5	Blank Solution	1250	90.9	224	64.34	−414	172.01
32	70				82.3	338	101.13	−445	180.29
33	75				73.0	464	119.48	−455	245.46
34	65	8.5	Blank Solution	1500	96.4	226	72.17	−425	171.06
35	70				84.5	328	105.98	−455	283.38
36	75				76.2	468	121.37	−460	319.73

with the values at pH 7.5 for the same conditions. However, in the experiments presented here, the measured Tafel slopes were very different from the expected 30–40 mV. The measured values are always higher than 120 mV. These values suggest that the metal surface could be covered by a film. Anodic dissolution of iron followed Tafel behavior for small overpotentials (slope 50–60 mV) and was not sensitive to speed of rotation. Tafel slope of the hydrogen evolution reaction is a function of pH value and temperature and it is not affected by speed of rotation conditions as it is a charge transfer property (Bala, 1988). Most of CO_2 corrosion reaction protective products and the coverage of the metal surface with the resulted scales caused b_a to decrease, further increasing in temperature and pH value may lead to further decreasing of b_a to a minimum values, then may lead to increase the value of b_a again. This indicates that the formation of protective film plays an important part in causing the decrease b_a (Hernandez et al., 2012). Also the changes in Tafel slopes (b_c & b_a) may be due either to removing of the protective film and/or to change in kinetic of dissolution of metal (Nor et al., 2011).

3.4. Characterization of the corroded surface

3.4.1. API X65 mild steel protective film thickness test

The protective film thickness is found from optical microscopy image of the cross-section as described in Fig. 11. The protective film data are listed in Table 11. Values of W_M in Table 11 are the weight of mild steel reacted in (mg/dm^2), and R_F is film ratio = W_{Film}/W_M.

Film porosity (ε) is calculated using the following expression:

$$W_M = \frac{W_1 - W_{wf}}{A} \tag{18}$$

where thickness of film is found from optical microscopy image of the cross-section, and thickness of 100% film is found out using the following calculations:

$$\text{thickness of 100\% dense film}(F_t) = \frac{\text{vol. of 100\% dense film} \times 10^4}{A} \tag{19}$$

where A is the surface area in dm^2 of the specimen and vol. of 100% film is found using:

$$\text{vol. of 100\% dense film} = \frac{W_f - W_{wf}}{\rho} \tag{20}$$

where W_f is the weight of the specimen with the film in gm, W_{wf} is the weight of the specimen after film removal (after cleaning) using chemical etching solution in gm, ρ is the density of a 100% $FeCO_3$ film (3.96 gm/cm^3). The surface area of the specimens used for weight loss measurements was 0.13 dm^2.

$$\varepsilon = 1 - \frac{91.944}{107.307} = 0.14$$

3.4.2. API X65 mild steel roughness test

The arithmetic average values of the roughness are listed in Table 12. During corrosion dissolution of the metal can lead to surface roughness and changes which can be taken into consideration. The roughness of corroded surface in absence of acetic acid is greater than that in presence of acetic acid because during the corrosion process, occur corrosion product formation on the corroded steel surface and a new phases is formed of a porous cementite (Fe_3C) layer and siderite $FeCO_3$ phase, while in absence of acetic acid a new phase is formed, i.e. siderite $FeCO_3$ phase. The source of the Fe_3C is probably the steel itself (Martin and Mokhtar, 2009), because, under the experimental conditions used, the formation of Fe_3C from iron and carbon dioxide is thermodynamically allowed (Martin and Mokhtar, 2009). The weight and dimensions of these phases are different from that of base metal that is already replaced by the non-protective and protective film formation. Eventually, the differences in roughness values measured in perpendicular directions are not the same, which indicates the shape of asperity in the two directions is not the same. Fig. 12 a–c shows the surface morphology and microstructure of non-corroded surface and corroded surface for corroded specimens of API X65 mild steel in CO_2-saturated, 3.5 wt % NaCl solution after 3 h at the optimum conditions in presence of acetic acid (presence of non-protective corrosion layer formation) and in absence of acetic acid (presence of protective corrosion layer formation) respectively. In Fig. 12c, it is clearly noticed that the rough surface in absence of acetic acid is higher than in presence of acetic acid due to the protective and non-protective corrosion layers formation created on the surface. The types of this layer appear as spherical or semi-spherical. Precipitation process depends on surface cleaning and the presence of a small amount of impurities (especially C) slows down the precipitation rate and determines the scale growth and its protectiveness of $FeCO_3$ and Fe_3C in these sites. These observations are also shown in Fig. 12b. Table 12, also shows the roughness measurement values for non-corroded surface and corroded surface of API X65 mild steel specimens in CO_2-saturated, NaCl environment in presence and absence of acetic acid at the optimum conditions. Martin and Mokhtar (Fang, 2006) proved that the roughness of corroded surface for BS-970 mild steel in absence of acetic acid and sodium acetate anhydrous in CO_2 saturated, 3% NaCl aqueous in turbulent flow conditions is greater than the roughness in presence of acetic acid and sodium acetate anhydrous.

3.4.3. API X65 mild steel X-Ray diffraction

X-ray diffraction (XRD) analyses results of the corroded surface

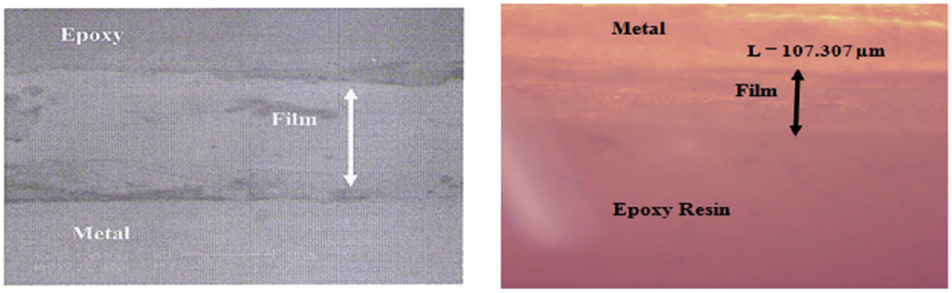

Fig. 11. SEM and Optical Microscopy of the Cross Sections of Corroded API X65 Mild Steel Specimen in CO_2-Saturated, 3.5 wt% NaCl Solution at the Optimum Conditions Showing the Thickness of the $FeCO_3$ Layer Formed.

Table 11
Experimental Runs for API X65 Mild Steel in CO_2-Saturated, 3.5 wt% NaCl Solution in Absence of Acetic Acid (Presence of the Protective Film Formation) by using the Optimum Conditions.

Run No.	W_1 (g)	W_f (g)	W_{wf} (g)	W_{Film} (mg/dm^2)	W_M (mg/dm^2)	R_F	Film thickness (F_t) μm
1	24.6301	24.6312	24.6265	36.15	27.69	1.31	91.297
2	24.8305	24.8311	24.8263	36.92	32.31	1.14	93.240
3	24.4471	24.4479	24.4432	36.15	30.00	1.21	91.297
Avg	24.6359	24.6367	24.6320	36.41	30.00	1.21	91.944

Table 12
Roughness Values for Corroded Surface of API X65 Mild Steel Specimens in CO_2–Saturated, 3.5 wt% NaCl Solution in Presence and Absence of Acetic Acid at the Optimum Conditions and Non Corroded Surface Specimens.

Not corroded surface μm	Corroded surface in presence of acetic acid μm	Corroded surface in absence of acetic acid μm
0.025	0.292	2.274
0.021	0.287	1.741
0.028	0.288	1.918
Average 0.025	0.289	1.978

(i.e., the corrosion product formed from the corroded surface) of API X65 mild steel specimens tested after exposure period 3 h at the optimum conditions (obtained in weight loss technique) in CO_2 saturated, 3.5 wt% NaCl solutions in presence and absence of acetic acid are shown in Fig. 13a and b. In Fig. 13 a, clearly revealed that there are new phases obtained on the surface of specimens in

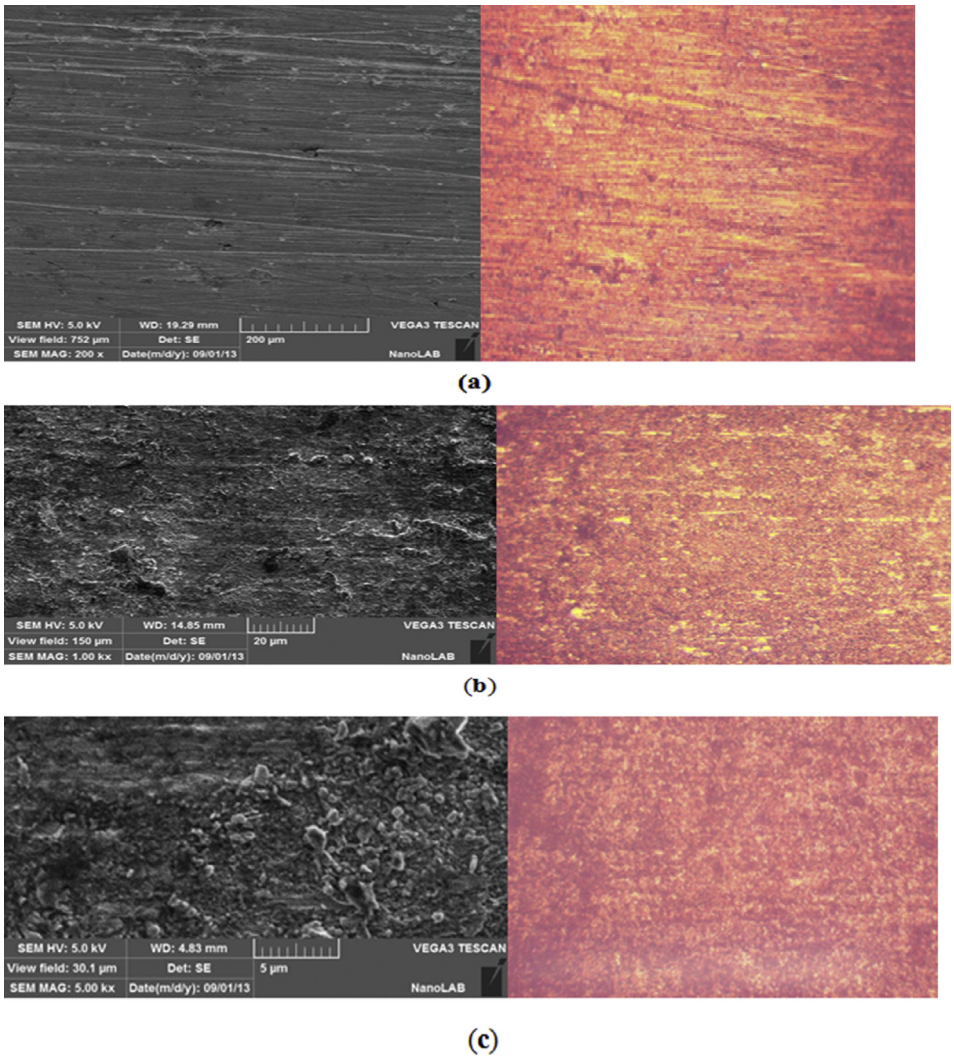

Fig. 12. Surface Morphology and Microstructure of Corroded API X65 Mild Steel Specimens in CO_2-Saturated, 3.5 wt% NaCl Solution at the Optimum Conditions: (a) Non Corroded Surface (b) Presence of Acetic Acid (Absence of Protective Film Formation) (c) Absence of Acetic Acid (Presence of Protective Film Formation).

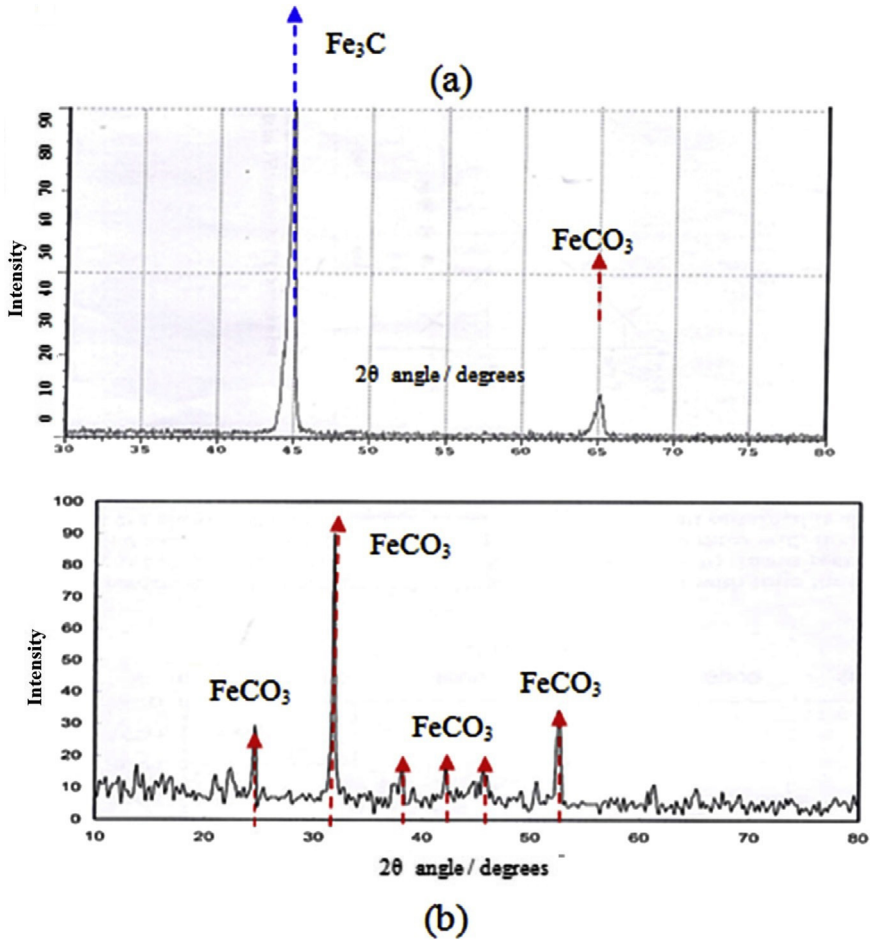

Fig. 13. XRD Pattern of Corroded API X65 Mild Steel Surface Specimens in CO_2-Saturated, 3.5 wt% NaCl Solution at the Optimum Conditions in: (a) Presence of Acetic Acid (Absence of Protective Film Formation) (b) Absence of Acetic Acid (Presence of Protective Film Formation).

presence of acetic acid (presence of the non-protective film formation) show that the scale consist of cementite Fe_3C and siderite ($FeCO_3$) phase while, phases obtained in absence of acetic acid (presence of the protective film formation) show that the scale consist of $FeCO_3$ phase only, as shown in Fig. 13 b. X-ray analysis data are described in Table 13. A peak near 30° 2θ is consistent with siderite ($FeCO_3$). $FeCO_3$ is the most important film that formed at carbon steel in sweet/CO_2 environment. This film can be function as a protective film for the carbon steel from the CO_2 corrosion. The film formation is strongly depending on the thermodynamics and kinetics of $FeCO_3$ precipitation. In principle, the precipitation process comprises two steps, nucleation, and particle growth. With increasing pH, making the rate decreased solubility of $FeCO_3$ resulting high deposition rate (Kermani and Morshed, 2003). The morphology of the film therefore depends on the dominating steps (Dugstad, 1998; Sun et al., 2003). Protective film formation is accelerated by measures that restrict the transport of reaction products from the surface (Dugstad et al., 2000). This comes in good agreement with Forero et al. (Forero et al., 2014) as he has studied the X-ray analysis of the corrosion scales formed on API 5L X70 and X80 steel pipe in deaerated 1% NaCl solution containing CO_2 and found the protective layer of ($FeCO_3$) film formed on the surface of both protective steels in the range 60–80 °C and observed the porous and discontinuous Fe_3C (from the steel microstructure) layer formed in the range of 40–60 °C.

3.4.4. API X65 mild steel hardness test

The Vickers micro-hardness testing (VMH) results are listed in Table 14. It is obvious that the hardness of corroded surface of API X65 mild steel in absence of acetic acid is higher than in presence it due to the presence of chemical compounds (Fe_3C and $FeCO_3$) formed of the corroded steel surface, these compounds ($FeCO_3$) increase the mechanical properties of the mild steel and increase the corrosion resistance and for less extent of compounds (Fe_3C). Table 14 also shows that the hardness of corroded surfaces in absence and presence of acetic acid is higher than that of uncorroded specimens. This refers to the great influence of the existence of iron carbide and ferrous carbonate on the hardness values in presence and absence of acetic acid respectively. Crolet et al. (Crolet et al., 1998) illustrate that the hardness of protected API X52, X60, X65 and X70 mild steel alloys are higher than unprotected specimens by precipitation process of an insoluble corrosion product $FeCO_3$ on CO_2 corrosion in turbulent flow conditions. This comes in good agreement with Ogundele and White (Ogundele and White, 1987) as he has studied the hardness of protected API-L80 steel and found greater hardness in comparison with the unprotected alloy specimens from corrosion of CO_2 saturated, brine solution using precipitated iron carbonate with and without influence of dissolved hydrocarbon gases and variable water chemistries.

Table 13
X-Ray Diffraction Pattern of Corroded API X65 Mild Steel Surface Specimen in CO_2-Saturated, 3.5 wt% NaCl Solution at the Optimum Conditions in Presence (Absence of Protective Film Formation) and absence (Presence of Protective Film Formation) of Acetic Acid.

Acid	Component	2θ (deg)	d-spacing (Å)	Intensity
Presence of acetic acid	Fe_3C	44.786	2.065	100
	$FeCO_3$	65.038	2.144	20
Absence of acetic acid	$FeCO_3$	24.023, 32.7765, 38.265, 43.399, 45.002, 46.1943, 52.243	1.738, 2.795, 1.965, 1.965, 1.965, 1.506, 1.732	30, 90, 20,20,20,14, 35

Table 14
Micro-Hardness Values for Corroded API X65 Mild Steel Surface Specimens in CO_2 –Saturated, 3.5 wt% NaCl Solution in Presence and Absence of Acetic Acid at the Optimum Conditions and Not Corroded Surface Specimens.

Not corroded surface micro-hardness Value VMH	Corroded surface in presence of acetic acid micro-hardness Value VMH	Corroded surface in absence of acetic acid micro-hardness Value VMH
135	184.8	307.8
134	180.0	269.6
138	182.2	291.7
136	181.5	280.9
137	183.0	287.7
Average 136	182.3	287.5

4. Conclusion

The second order polynomial regression analysis of the objective function (corrosion rate) describes the behavior of the process in both absence and presence of the protective film. The corrosion rate of API X65 mild steel in CO_2 saturated, 3.5 wt % NaCl solution in presence and absence of acetic acid, increases with increasing temperature, acetic acid concentration and speed of rotation, and decreased with increasing solution pH. The primary corrosion product of API X65 mild steel is ferrous carbonate ($FeCO_3$) at high temperatures, high pH's (alkaline media) and absence of acetic acid, which could act as a protective film so that CO_2 corrosion rate can be reduced. The corrosion current densities in presence and absence of acetic acid increase with increasing temperature and speed of rotation and decrease with increasing pH value in absence of acetic acid.

Acknowledgment

The authors would like to thank Chemical Engineering Department – College of Engineering - Baghdad University.

References

Aprael, A.S., Khadom, A.A., Ibraheem, H.F., 2011. Peach juice as an anti-corrosion inhibitor of mild steel. Anti-Corros. Methods Mater. 58, 116–124.
Bagotsky, V.S., 2006. Fundamentals of Electrochemistry, second ed. John Wiley & Sons, Inc.
Bala, H.B., 1988. Electrochemical investigation of corrosion of iron in oxygen saturated sulphuric acid solutions. Br. Corros. Jr. 23, 29–36.
Box, H., Hunto, 2005. Statistics for Experiments, second ed. John-Wiley and Sons.
Crolet, J.L., Thevenot, N., Nesic, S., 1998. Role of conductive corrosion products in the protectiveness of corrosion layers. Corrosion 54, 194–203.
Dougherty, J.A., 2004. Annual Corrosion Conference. No. 4376. NACE.
Dugstad, A., 1998. Mechanism of Protective Film Formation during CO_2 Corrosion of Carbon Steel, Corrosion, vol. 98. NACE, Houston, Texas.
Dugstad, A., Hammer, H., Seirstein, M., 2000. Effect of steel microstructure upon corrosion rate and protective iron carbonate film formation. Corrosion 23, 1–15.
Fang, H., 2006. Low Temperature and High Salt Concentration Effects on General CO2 Corrosion for Carbon Steel. M.Sc. Thesis. The Russ College of Engineering and Technology of Ohio University, Ohio, USA.
Forero, A.B., Nunez, M.M.G., Bott, I.S., 2014. Analysis of the corrosion scales formed on API 5L X70 and X80 steel pipe in the presence of CO_2. Mater. Res. 17, 461–471.
Frankel, G.S., 2004. Localized corrosion of metals; a review of the rate controlling factors in initiation and growth, Fontana corrosion Center. Electrochem. Soc. Proc. 99, 42.
Gabe, D.R., Makanjoula, P.A., 1986. Electrochemical Engineering. EFCF Publication Series No. 15. In: AIChE Symposium Series, vol. 98, p. 309.
Garsany, Y., Pletcher, D., Hedges, B., 2002. The role of acetate in CO_2 corrosion of carbon steel. Corrosion 2273, 1–16.
George, K.S., 2003. Electrochemical Investigation of Carbon Dioxide Corrosion of Mild Steel in the Presence of Acetic Acid. M.Sc Thesis. Ohio University, USA.
George, K.S., Nesic, S., 2007. Investigation of carbon dioxide corrosion of mild steel in the presence of acetic acid-part 1: basic mechanisms. Corrosion 63.
Gulbrandsen, E., Nesic, S., Stangeland, A., Buchardt, T., Sundfaer, B., Hesjevik, S.M., Skjerve, S., 1998. Effect of precorrosion on the performance of inhibitors for CO_2 corrosion of carbon steel. Corrosion 13.
Gunaltum, Y.M., Larrey, D., 2000. Correlation of Cases of Top of Line Corrosion with Calculated Water Condensation Rates. Corrosion, No. 71. NACE, Houston, Texas.
Hedges, B., McVeigh, L., 1999. The Role of Acetate in CO_2 Corrosion: the Double Whammy. Corrosion, No. 12. NACE, Houston, Texas.
Hernandez, J., Munoz, A., Genesca, J., 2012. Formation of iron-carbonate scale-layer and corrosion mechanism of API X70 pipeline steel in carbon dioxide-saturated 3% sodium chloride. Corrosion 10, 251–258.
James, A.D., 2004. A Review of the Effect of Organic Acids on CO_2 Corrosion. Corrosion, 04376. NACE, Houston, Texas.
Jeff Wu, C.F., Michael, S.H., 2009. Experiments: Planning, Analysis and Optimization, second ed. John Wiley and Sons, Inc., New York, USA.
Jezmar, J., 2002. Monitoring methods of cathodic protection of pipe lines. Corros. Meas. 2, 1–13.
Jiabin, H., William, J.C., Jinsou, Z., 2011. Effect of sodium chloride on corrosion of mild steel in CO_2-saturated brines. J. Appl. Elect. 41, 741–750.
Joosten George, I., Omkar, N., Nafday, A., 2004. Film Formation and CO_2 Corrosion in the Presence of Acetic Acid. Master theses of Fritz, j., Dolores, and Russ, H. College of Engineering and Technology, Ohio University.
Kermani, M.B., Morshed, A., 2003. Carbon dioxide corrosion in oil and gas production-A Compendium. Corrosion 59, 659–683.
Koteeswaran, M., 2010. CO_2 and H_2S Corrosion in Oil Pipeline. University of Stavenger, p. 79.
Marcus, P., Herbelin, J.M., 1993. Corros. Sci. 34. No. 1123.
Martin, C.F., Mokhtar, C.I., 2009. Effect of low concentration acetic acid on CO_2 corrosion in turbulent flow conditions. Corrosion 34, 129–146.
Mokhtar, I.C., 2005. Prediction CO_2 Corrosion with the Presence of Acetic Acid. UMIST, United Kingdom. Ph.D. Thesis.
Nervana, A.A., 2010. The effect of temperature and pH on the corrosion rate of carbon steel in 1 M NaCl. Al-Taqani 24, 128–138.
Nesic, S., 2007. Key issues related to modelling of internal corrosion of oil and gas pipelines – a review. Corros. Sci. 49 (12), 4308–4338.
Nor, A.M., Suhor, M.F., Mohamed, M.F., Singer, M., Nesic, S., 2011. Corrosion of Carbon Steel in High CO_2 Environment: Flow Effect. Corrosion, No. 11242. NACE, pp. 1–18.
Nyborg, R., 2010. CO_2 corrosion models for oil and gas production systems. Corrosion 10371, 1–20.
Ogundele, G., White, W., 1987. Observations on the influence of dissolved hydrocarbon gases and variable water chemistries on corrosion of an API-L80 steel. Corrosion 43, 665–673.
Roberge, P., 2012. Handbook of Corrosion Engineering, second ed. McGraw-Hill., Inc.
Shrier, L.L., Jarman, R.A., Burstein, G.T., 2000. Corrosion Control, third ed., vol. 2
Sun, Y., George, K., Nesic, S., 2003. The Effect of Cl^- and Acetic Acid on Localized CO_2 Corrosion in Wet Gas Flow. Corrosion, No. 3327. NACE.
Tran, T., Brown, B., Nesic, S., 2013. Investigation of the Mechanism for Acetic Acid Corrosion of Mild Steel. Corrosion, No. 2487. NACE.
Uhlig, H.H., 2011. Corrosion Handbook, third ed. John-Wiley and Sons, Inc.
Uhlig, H.H., 2013. Handbook on Chemical Etching. John-Wiley and Sons Inc.
Uhlig, H.H., Winston, R.R., 2008. Corrosion and Corrosion Control, fourth ed. John-Wiley and Sons Inc.
Zhang, G., Cheng, Y., 2009. On the fundamentals of electrochemical corrosion of X65 steel in CO_2-containing formation water in the presence of acetic acid in petroleum production. Corros. Sci. 51, 87–94.